# First-principles study of the large-gap three-dimensional topological insulators $M_3Bi_2$ ($M$ = Ca, Sr, Ba)

Ronghan Li, Qing Xie, Xiyue Cheng, Dianzhong Li, Yiyi Li, and Xing-Qiu Chen*
*Shenyang National Laboratory for Materials Science, Institute of Metal Research, Chinese Academy of Science, 110016 Shenyang, Liaoning, China*
(Received 28 September 2015; revised manuscript received 8 November 2015; published 30 November 2015)

By means of first-principles calculations in combination with universal evolutionary structure search, we identified the crystalline structure of long-term argued $M_3Bi_2$ ($M$ = Sr, Ca, and Ba), which crystallizes in a tubelike structure stacked by buckled graphenelike layers. The analyses of electronic structures revealed that this type of $M_3Bi_2$ is a native wide-gap three-dimensional topological insulator with the inverted band order induced mainly by crystal field effect. The spin-orbit coupling effect was found to open the band gap and further enhance the band inversion. Among them, $Sr_3Bi_2$ is most attractive due to its largest fundamental gap of about 0.3 eV and the directly inverted band gap of 0.81 eV at Γ obtained within the framework of Green functionals ($GW$). Moreover, the computation also evidences that their tubelike structure is suitable for further treatment via magnetic dopants, which prefer to occupy 1$b$ site. Interestingly, the ferromagnetic insulating state has been achieved for V- and Mn-doped cases. This may provide a further opportunity to observe the quantized anomalous Hall effect in its thin films.

DOI: 10.1103/PhysRevB.92.205130 PACS number(s): 71.20.Nr, 71.20.Eh

Within recent years, topological materials, including topological insulators (TIs) [1,2], topological crystalline materials (TCIs) [3], topological (Dirac) semimetals [T(D)Ss] [4–10], topological Wely semimetals (TWSs) [4,11–13], topological Wely line-node (or node-line) semimetals (TWLSs) [13–16], as well as topological metals (TMs) [17,18], have become extensively interesting not only for condensed matter physics and materials science but also for fundamental Dirac fermions. Because the metal element of bismuth offers a very strong spin-orbit coupling effect and easily induces so-called band-inversion occurrence, which are significant for the nontrivial topological states, most of topological materials basically consist of bismuth in its $Bi^{3+}$ valence state, such as $Bi_2(Se,Te)_3$, $Bi_{2-x}Te_{3-y}Se_y$, $TlBi(Se_{1-x}S_x)$, $Bi_2(Te,Se)_2(Se,S)$, $PbBi_4Te_7$, $Pb_nBi_2(Se,Te)_{n+3}$, $A^{III}BiO_3$ ($A^{III}$ = Al, Ga, In, Sc, Y, and La), $Pb_5Bi_{24}Se_{41}$, $Ge_2X_2Te_5$ ($X$ = Sb and Bi), and $Bi_3Te_4I$ [19–32]. Recently, the compound of $BaBiO_3$ [33], with the mixed-valences states between $Bi^{3+}$ and $Bi^{5+}$, was reported to exhibit a large topological energy gap of 0.7 eV only in its electron-doped region. From the viewpoint of chemical formation, in order to form a $Bi^{3+}$ configuration in a topological material, it will need other constituents having larger electronegativity than that of Bi, such as Se, Te, O, S, C, Pb, F, Cl, Br, I, etc. Within this situation, Bi lose its three $p$ valence electrons in the form of the fully unoccupied Bi-$p$-orbits states. Even TI was also found with a valence state of $Bi^{1+}$ in the single-layer structural form of $Bi_4Br_4$ [34,35] and with a zero valence state in the pure bismuth metal via a doping of $Sb(Bi_xSb_{1-x})$ [36,37]. Interestingly, in some topological materials Bi even has its $Bi^{3-}$ valence state, such as the antiperovskite TIs or TCIs of $M_3NBi$ ($M$ = Ca, Sr and Ba) [38,39] and LaPtBi [40,41], TDSs of $A_3Bi$ ($A$ = Na, K, and Rb) [6,42–44], and TMs of $M_2NBi$ ($M$ = La, Nd) [18]. This negative valence state of Bi can be attributed to the fact that the electronegativity of the constituents (i.e., alkaline-earth and alkali-metal elements) in a compound are much lower than that of bismuth and Bi would obtain three valence electrons to form its fully filled $p$ orbits. Naturally, given such a simple concept to form a fully filled $p$ orbital in the $Bi^{3-}$ valence state, it is highly interesting to know whether the composition of $M_3Bi_2$ ($M$ = Ca, Sr, and Ba) also exists and, if yes, whether they also exhibit a similar topological feature?

In fact, the $M$-Bi binary systems ($M$ = Sr, Ca, and Ba) were extensively studied since the 1950s and the compounds of $M_3Bi_2$ were quite often reported in the literature [45–58]. $Mg_3Bi_2$ has been proved as a narrow gap semiconductor in as early as 1975 [59]. However, to date the details of the crystalline structures of those compounds of $M_3Bi_2$ have still remained unknown. Through first-principles calculations in combination with evolutionary structural searches, we have identified the $hR45$ structural details of $M_3Bi_2$. The analysis of the electronic structures reveals that they are the three-dimensional TIs. In particular, the compound of $Sr_3Bi_2$ is a wide-gap 3D-TI with a wide fundamental band gap of about 0.3 eV and a highly large inverted direct gap of 0.8 eV at Γ naturally induced by the crystal-field splitting. The spin-orbit coupling effect (SOC) was found to open the gap and further enhance its band inversion. Due to the special tubelike structure, our calculations revealed that $Sr_3Bi_2$ is suitable for further doping treatment with transition metal elements (i.e., V and Mn) to obtain a ferromagnetic insulating state. This fact may provide a chance to observe a quantized anomalous Hall effect.

In order to identify the existence of $M_3Bi_2$, we have performed the compositional and structural searches on these binary systems via VASP [60,61] with projector-augmented-wave (PAW) pseudopotentials [62] and Perdew-Burke-Ernzerhof (PBE) exchange and correlation functionals [63], in combination with the variable-compositional technique supplemented in USPEX [64–66] within the framework of density functional theory (DFT) [67,68]. A very accurate optimization of

*Corresponding author: xingqiu.chen@imr.ac.cn

 

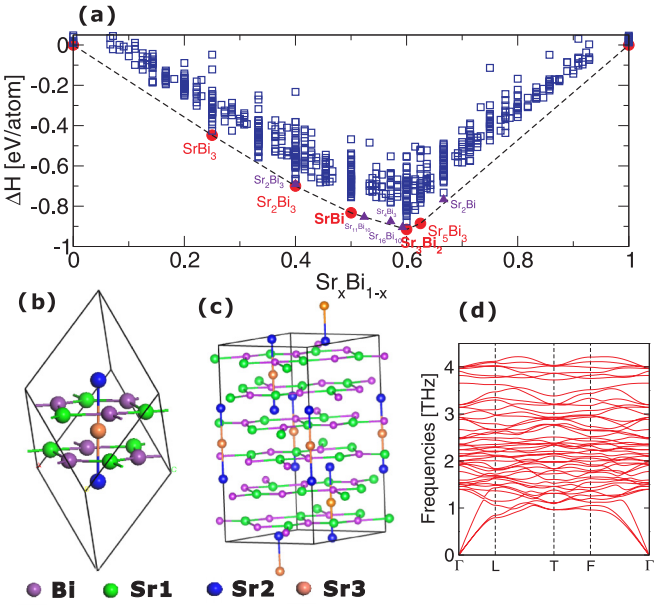


FIG. 1. (Color online) The derived GGA-type PBE enthalpies of formation predicted by variable-composition evolutionary computations for the Sr-Bi system (for more details refer to Table S1 of the Supplemental Materials [73]). Every square represents an individual structure and the most stable ground state phases (solid circles) are connected to a convex hull. Hollow squares denote metastable phases above the convex hull. In (b), (c), and (d) are the primitive cell, the unit cell of $Sr_3Bi_2$, and the derived phonon dispersion, respectively. In its optimized primitive cell, $Sr_3Bi_2$ crystallizes in the rhombohedral structure (space group of $R\bar{3}$, No. 148), having a lattice constant of $a = 9.1353$ Å and the rhombohedral angle of 66.157° with Bi at 6*f* site (0.09161, 0.44524, 0.70241), Sr1 at 6*f* site (0.37391, 0.08406, 0.81051), Sr2 at 2*c* site (0.31983, 0.31983, 0.31983), and Sr3 at 1*b* site (0.5, 0.5, 0.5).

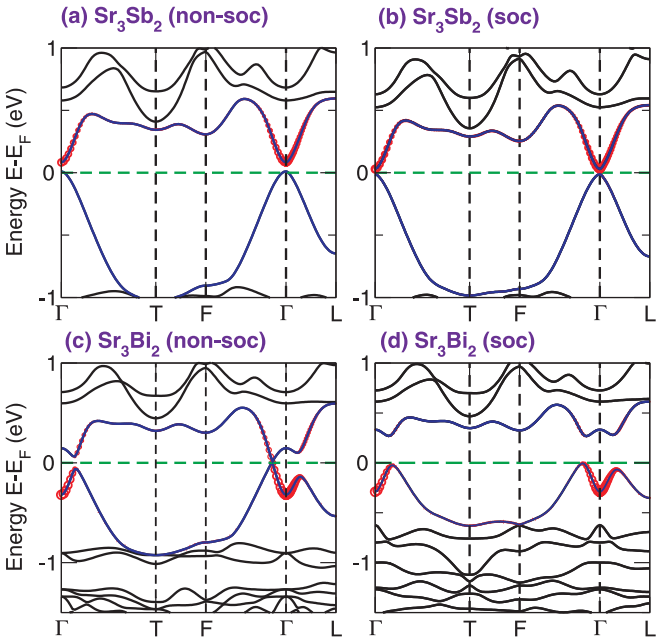


FIG. 2. (Color online) Calculated electronic band structures of $Sr_3Bi_2$ in comparison with the isoelectronic and isostructural $Sr_3Sb_2$. (a) and (b) $Sr_3Sb_2$ without and with the SOC inclusion, respectively. (c) and (d) $Sr_3Bi_2$ without and with the SOC inclusion, respectively. Note that the red solid circles denote the Bi *s*-like states.

structural parameters was achieved by minimizing forces (below 0.0001 eV/Å). Electronic properties are calculated with 350 eV plane-wave energy cutoff and $11 \times 11 \times 11$ grid *k* mesh. The phonon spectra is derived with the code of Phonopy [69] within the framework of finite-displacement approach and density functional perturbation theory (DFPT) [70] in a Born-Karman boundary condition in a supercell containing $2 \times 2 \times 2$ primitive cells. The projected surface states are obtained from maximally localized Wannier functions within a linear combination of atomic orbits (LCAO) method [71] in tight-binding approximation by employing Wannier90 code [72]. For the studies on the magnetic substitutions, we performed spin-polarized calculations for $Sr_3Bi_2$ doped with various transition metal elements, using a 120-atom supercell with two of the nearest Sr3 atoms substituted by a magnetic dopant. The crystal structure and the magnetic state are fully optimized to obtain the ground state.

As illustrated in Fig. 1(a) for the Sr-Bi system, the computation reveals a convex hull showing five stable ground-state compounds, $SrBi_3$, $Sr_2Bi_3$, SrBi, $Sr_3Bi_2$, and $Sr_5Bi_3$. According to the convex hull, four important facts can be outlined here: (i) compounds of $SrBi_3$ and $Sr_5Bi_3$ are in nice agreement with the experimental observation with both structures and compositions, (ii) SrBi crystalizes in a hexagonal $P6_3/mc$ phase [73], which is an ever-reported but structurally not-yet resolved compound [45], (iii) three metastable compositions of $Sr_2Bi$, $Sr_3Bi_4$, and $Sr_2Bi_3$ lie above the convex hull, but their calculated structure agrees well with the experimentally observed one, and (iv) a lowest-enthalpy composition of $Sr_3Bi_2$, which is also an ever-reported but structurally not-yet resolved phase, crystallizes in the *hR*45 structure. It needs to be emphasized that our USPEX search did not find more stable structure than that of another two experimentally reported compositions of $Sr_{11}Bi_{10}$ and $Sr_{16}Bi_{11}$. In addition, their enthalpies of formation are all slightly above the convex hull, which is shown in Fig. 1(a). As illustrated in Figs. 1(b) and 1(c), the structure of $Sr_3Bi_2$ is highly special, because of its tubelike shape stacked by the slightly buckled Sr/Bi graphenelike layers interacting with the centered Sr-atom chain in each tube. Each Sr/Bi graphenelike layer preserves the threefold rotation symmetry. Furthermore, the derived phonon dispersion of $Sr_3Bi_2$ was further demonstrated to be dynamically stable, as evidenced in Fig. 1(d). In similarity, for both Ca-Bi and Ba-Bi binary systems, our calculations also found the stable composition of $Ca_3Bi_2$ and $Ba_3Bi_2$ with the same *hR*45 structure at their ground states, respectively (refer to Table S3 of the Supplemental Materials [73]).

Besides a special structure, $Sr_3Bi_2$ exhibits very interesting electronic properties. The calculated bulk band structures along the high symmetry lines in the Brillouin zone (BZ) for $Sr_3Bi_2$ are shown in Figs. 2(c) and 2(d). Without SOC, $Sr_3Bi_2$ is semimetal with a gapless three-dimensional (3D) Dirac cone located in the vicinity of the Γ point along the $F$-Γ line. It can be seen that $Sr_3Bi_2$ exhibits a typical band anticrossing feature, with the top of the valence band and the bottom of the conduction band at Γ, which is primarily

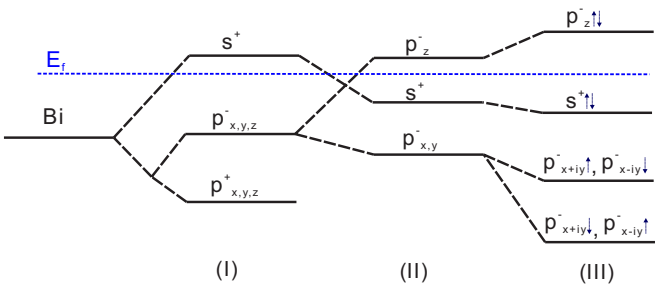


FIG. 3. (Color online) Schematic diagram of the evolution from the atomic orbitals of Bi into the conduction and valence bands of $Sr_3Bi_2$ at the Γ point. The three different steps (I), (II), and (III) represent the effect of turning on chemical bonding, crystal-field splitting, and SOC, respectively. The blue line denotes the Fermi energy level schematically.

composed of Bi *s*-like and Bi *p*-like states, respectively. With SOC inclusion, significant changes have been observed. First, $Sr_3Bi_2$ becomes a relatively wide-gap insulator (with a fundamental indirect gap of 0.28 eV) by splitting the 3D Dirac cone. Second, the inverted band gap at Γ is substantially increased to 0.62 eV due to the enhanced band inversion caused by SOC. It can be seen that the inverted band ordering is driven not solely by SOC, chemical bonding and crystal field also make great contributions. As a comparison, we also plot the bulk band structures of the isostructural and isoelectronic artificial compound of $Sr_3Sb_2$, as illustrated in Figs. 2(a) and 2(b), whether including SOC or not, $Sr_3Sb_2$ is a narrow-gap insulator without inverted band ordering. However, by expanding the crystal volume to a certain degree, $Sr_3Sb_2$ exhibits an inverted band, showing a similar feature to $Sr_3Bi_2$, which further supports this crystal-field causing band inversion. To get a better understanding of the inversion and the parity exchange, here we have plotted a brief schematic to interpret the band evolution from initial atomic orbitals to final inverted band order at the Γ point in Fig. 3. Since the states near the Fermi surface are mainly coming from the orbitals of Bi, we neglected the effect of other orbitals. Its evolution has been summarized in three steps (I), (II), and (III). In step (I) the chemical bonding occurs among Bi and Sr atoms, which results in two states ($p^-_{x,y,z}$ and $p^+_{x,y,z}$) of each Bi *p* orbital according to their parities. In step (II), after switching on the crystal field, these $p_{x,y,z}$ orbitals are further split into both $p_{x,y}$ and $p_z$ due to the threefold axis symmetry. Indeed, this step causes a band inversion between $s^+$ and $p_z^-$ at the Γ point. Finally, in step (III) the SOC inclusion further splits the energy levels, enhancing the band inversion. In particular, it needs to be emphasized that the identification of the band-inverted feature on the basis of conventional DFT may lead to false-positive assignment if the band-inversion strength is not large enough, due to the well-documented band-gap underestimation problem. For this reason we have revisited the electronic dispersion of $Sr_3Bi_2$ by *GW* method [74–76], which indeed yields the substantially same physical picture. Fortunately, for $Sr_3Bi_2$ our *GW* calculations obtain a fundamental gap of 0.31 eV and a larger inverted band gap of 0.81 eV at Γ.

The fact that the band inversion of $Sr_3Bi_2$ occurs only once at the Γ point and is not driven alone by SOC, is suggestive of the formation of a nontrivial topological state. In order to provide further support, we have analyzed the evolution of the band gap as a function of the lattice constant for $Sr_3Bi_2$. According to our calculations, a topological phase transition of $Sr_3Bi_2$ from a topologically nontrivial to a trivial state occurs with increasing the volume, in nice agreement with the obvious fact that any insulator is topologically trivial in the atomic limit. In addition to the band inversion, an alternative way to identify TI states is the parity criteria proposed by Fu and Kane [77,78]. Considering that the $R\bar{3}$ phase possesses the inversion symmetry, this criteria can be applied and serves as further support for our analysis. The product of the parities of the Blöch wave function for the occupied bands at time-reversal invariant momenta (TRIMs) of threefold degenerated *L* ($\pi$,0,0), threefold degenerated *F* ($\pi$, $\pi$, 0), single *T* ($\pi$, $\pi$, $\pi$) has been derived to be (+) for both $Sr_3Bi_2$ and $Sr_3Sb_2$. Therefore, these seven TRIMs display a positive (+) global parity. At Γ the situation is different: the product of the parities is + or − depending on whether or not the band inversion occurs. Our analysis reveals a negative (−) parity product at Γ for $Sr_3Bi_2$, whereas a positive (+) parity product occurs for $Sr_3Sb_2$. We can therefore trustfully conclude that $Sr_3Bi_2$ is a native topological nontrivial insulator with $Z_2$ index (1; 000). Our further calculations for $Ca_3Bi_2$ and $Ba_3Bi_2$ suggest that they have qualitatively the same topological properties as $Sr_3Bi_2$ does (refer to Fig. S1 of the Supplemental Materials [73]).

Furthermore, we have produced the intrinsic properties of the topological phase in $Sr_3Bi_2$, and provide further evidence of this TI state by inspecting the surface properties. We have computed the surface band dispersions for the (001) and (111) surfaces using the *ab initio* TB model. The *ab initio* TB model is constructed by downfolding the bulk energy bands, obtained by first-principles calculations, using maximally localized Wannier functions (MLWFs). As the bulk energy bands near Fermi energy are predominantly formed by hybridized *s*- and *p*-like Bi orbitals, the MLWFs are derived from atomic *s*- and *p*-like orbitals and the TB parameters are determined from the MLWFs overlap matrix. The TB bulk bands perfectly reproduce the DFT bands around the Fermi energy $E_F$ up to $\sim\pm3$ eV. The surface band structures have been calculated by adopting two slabs for the (001) and (111) surfaces with thickness of 150 and 180 atomic layers, respectively. The results of the TB calculations are summarized in Fig. 4. These results evidence clearly that the (001) and (111) surfaces posses spin-resolved helical metallic surface states which cross each other forming a single Dirac cone, in nice agreement with the analysis of the parity and the band inversion.

Interestingly, it has been noted that such a tubelike structural feature in these three compounds of $M_3Bi_2$ is indeed suitable for doping treatment. The most fascinating aspect would be to break the time-reversal symmetry of $Sr_3Bi_2$ by introducing ferromagnetism, which can naturally lead to the quantized anomalous Hall (QAH) effect [79–83]. For sake of this aim, we have systematically performed the calculations by considering the 3*d*, 4*d*, and 5*d* transition metals to substitute different sites in $Sr_3Bi_2$. It has been found that those metals all prefer to occupy the 1*b* site of Sr3 atom and the substitutional energies of 3*d*-series transition metal atom have been shown in Fig. 5(a). The spin-polarized calculations demonstrated that

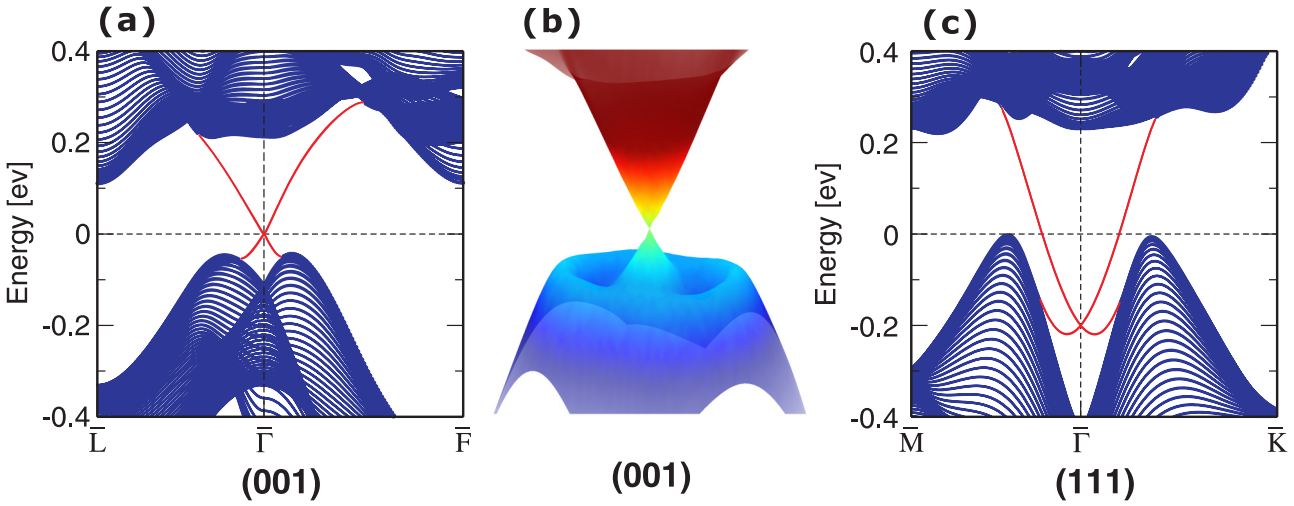


FIG. 4. (Color online) (a) and (c) TB energy band structures of the (001) and (111) surfaces in the primitive cell of $Sr_3Bi_2$, respectively. The appearance of the gapless Dirac-cone-like metallic states evidences the occurrence of TI. Plane (b) is a 3D picture to illustrate the Dirac cone in the 2D (001) surface.

these dopants all carry the local large magnetic moments and the ferromagnetic states are energetically favorable by highly large magnetization energies as compared with their corresponding antiferromagnetic states, as illustrated in Fig. 5(b). In particular, the calculations demonstrated that an insulating ferromagnetic state has been already obtained for 3*d*-V (with a spin-polarized ferromagnetic energy of 1.50 eV) and 3*d*-Mn (with a spin-polarized ferromagnetic energy of 2.64 eV), whereas the states are metallic or half-metallic for all other

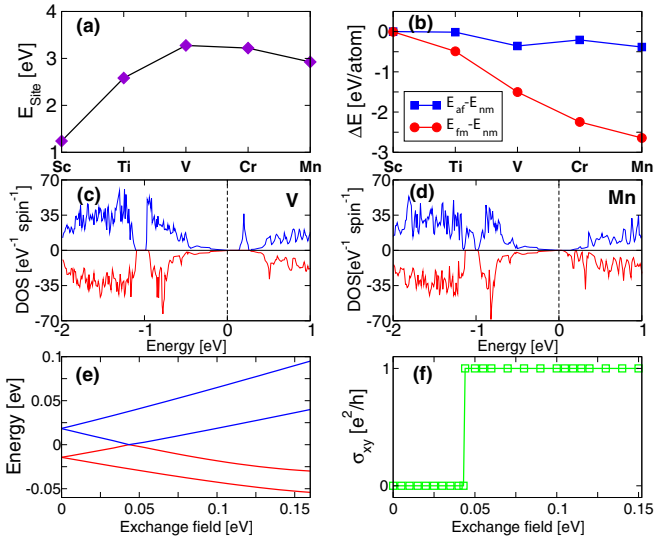


FIG. 5. (Color online) (a) The derived site preference energies of transition metal by substituting Sr3 atom in $Sr_3Bi_2$. (b) The spin-polarized energies induced by magnetic dopants. (c) and (d) Total densities of states (DOSs) for 3*d*-V and 3*d*-Mn doped cases, respectively. (e) The lowest subbands at the Γ point plotted versus the exchange field for $Sr_3Bi_2$ films with thickness of 25 atomic layers along the [111] direction. (f) The derived Hall conductance for this thin film. The Hall conductance is zero before the QAH transition but $\sigma_{xy} = \frac{e^2}{h}$ afterward.

doping cases. To obtain a ferromagnetic insulating state for TIs is important for the appearance of QAH. Mechanically, it is clear that because of the Hund's rule coupling of 3*d* transition ions the high-spin state can be expected for these magnetic dopants. Because these magnetic dopants substitute Sr atom, it can be reasonably expected that they should be in 2+ valence state. For V and Mn ions, the 2+ valence state makes them have three and five 3*d* electrons, respectively. For the V-doped case, the high-spin state of the electronic configuration should be in the configuration of $t_{2g}^{3\uparrow} e_g^{0\uparrow} t_{2g}^{0\downarrow} e_g^{0\downarrow}$. In fact, the local coordination of $V^{2+}$ exactly provides such a possibility because it sites at a shared vertex of two tetrahedra formed by its six nearest neighboring $Bi^{3-}$ ions. Such a local crystal field splits the *d* shell into $t_{2g}$ and $e_g$ manifolds. Within this situation, the V dopant in $Sr_3Bi_2$ can result in a gap between $t_{2g}$ and $e_g$ manifolds, evidencing the occurrence of the ferromagnetic insulating state as shown in Fig. 5(c). For the Mn-doped case, in its high-spin state the electronic configuration favors in energy the unpaired $d^{5\uparrow} d^{0\downarrow}$ one. This will result in the occurrence of the insulating state of the Mn-doped case, as evidenced by a gap between spin-up and spin-down density of states in Fig. 5(d). However, for other magnetic dopants there is no way to obtain the insulating state in their high spin states due to the limitation of the local coordination around the Sr3 atom. Once the ferromagnetic order is achieved in TI, the QAH effect can be realized in its 2D thin films [79]. We added a variant of the Zeeman effect to our original TB model Hamiltonian of the thin film to describe the relationship between the energy of the lowest subbands at Γ and the exchange field, and the obtained result is further elucidated in Fig. 5(e). It is clear that a strong exchange field will certainly induce the QAH transition, because it increases the energy of the highest valence band and, simultaneously, reduces the energy of the lowest conduction band. This behavior is mainly due to the fact that the Pauli matrix $\sigma_z$ in the exchange field shows an opposite sign to the Zeeman coupling terms in the effective Hamiltonian. Thus, the crossing between these two bands will be accepted as long as the exchange feld is strong enough. The occurrence of their

crossing implies the change of the Chern number of one of the subbands, thereby causing QAH transition as illustrated in Fig. 5(f), in which the Hall conductance can be derived from the formula

$$\sigma_{xy} = \frac{e^2}{h}\frac{1}{2\pi}\iint d_{kx}d_{ky}F_{xy}(k) = \frac{e^2}{h}n, \quad (1)$$

where

$$n = \frac{1}{2\pi}\iint d_{kx}d_{ky}F_{xy}(k) \quad (2)$$

is the winding number of the gauge transformation on the boundary of the piecewise definition of the wave functions, and $F_{xy}(k)$ is the Berry curvature. Figure 5(f) shows that an integer Hall conductance occurs above the exchange field of 0.044 eV for the $Sr_3Bi_2$ thin film with the 25 atomic layers along the [111] direction (corresponding to the [0001] direction of the conventional unit cell). With further increasing the thickness of the thin film, the exchange field can be reduced for the onset of the QAH transition.

In summary, by means of first-principles calculations in combination with universal structural searches, we have refined the detailed structure of the long-term argued compound of $Sr_3Bi_2$, which crystallizes in a rhombohedral structure (space group of $R\bar{3}$, No. 148). The calculations demonstrated that $Sr_3Bi_2$ is a three-dimensional TI with a wide band gap of about 0.3 eV and a highly large inverted direct gap of 0.8 eV at Γ naturally induced by the crystal-field splitting. The SOC effect plays an important role to open its band gap and further enlarge its band inversion. The surface spin-resolved states and the presence of Dirac cone have been evidenced. Moreover, $Sr_3Bi_2$ is suitable for further doping treatment with transition metal elements (i.e., V and Mn) to obtain a ferromagnetic insulating state. It also needs to be mentioned that both $Ca_3Bi_2$ and $Ba_3Bi_2$ exhibit similar topological properties.

This study was supported by the "Hundred Talents Project" of the Chinese Academy of Sciences and from the Major Research Plan (Grant No. 91226204), the Key Research Program of Chinese Academy of Sciences (Grant No. KGZD-EW-T06), the NSFC of China (Grants No. 51474202 and No. 51174188) and Beijing Supercomputing Center of CAS (including its Shenyang branch) as well as the high-performance computational cluster in the Shenyang National University Science and Technology Park.

[1] M. Z. Hasan and C. L. Kane, Rev. Mod. Phys. **82**, 3045 (2010).
[2] X. L. Qi and S. C. Zhang, Rev. Mod. Phys. **83**, 1057 (2011).
[3] L. Fu, Phys. Rev. Lett. **106**, 106802 (2011).
[4] X. Wan, A. M. Turner, A. Vishwanath, and S. Y. Savrasov, Phys. Rev. B. **83**, 205101 (2011).
[5] S. M. Young, S. Zaheer, J. C. Y. Teo, C. L. Kane, E. J. Mele, and A. M. Rappe, Phys. Rev. Lett. **108**, 140405 (2012).
[6] Z. J. Wang, Y. Sun, X.-Q. Chen, C. Franchini, G. Xu, H. Weng, X. Dai, and Z. Fang, Phys. Rev. B. **85**, 195320 (2012).
[7] S-Y. Xu, C. Liu, S. K. Kushwaha, R. Sankar, J. W. Krizan, I. Belopolski, M. Neupane, G. Bian, N. Alidoust, T.-R. Chang, H.-T. Jeng, C.-Y. Huang, W.-F. Tsai, H. Lin, P. P. Shibayev, F.-C. Chou, R. J. Cava, and M. Z. Hasan, Science **347**, 294 (2015).
[8] Z. K. Liu, B. Zhou, Y. Zhang, Z. J. Wang, H. M. Weng, D. Prabhakaran, S.-K. Mo, Z. X. Shen, Z. Fang, X. Dai, Z. Hussain, and Y. L. Chen, Science **343**, 864 (2015).
[9] Z. K. Liu, J. Jiang, B. Zhou, Z. J. Wang, Y. Zhang, H. M. Weng, D. Prabhakaran, S-K. Mo, H. Peng, P. Dudin, T. Kim, M. Hoesch, Z. Fang, X. Dai, Z. X. Shen, D. L. Feng, Z. Hussain, and Y. L. Chen, Nat. Mater. **13**, 677 (2014).
[10] T. Liang, Q. Gibson, M. N. Ali, M. Liu, R. J. Cava, and N. P. Ong, Nat. Mater. **14**, 280 (2015).
[11] S.-M. Huang, S.-Y. X, I. Belopolski, C.-C. Lee, G. Q. Chang, B. K. Wang, N. Alidoust, G. Bian, M. Neupane, C. L. Zhang, S. Jia, A. Bansil, H. Lin, and M. Z. Hasan, Nat. Commun. **6**, 7373 (2015).
[12] H. Weng, C. Fang, Z. Fang, B. A. Bernevig, and X. Dai, Phys. Rev. X **5**, 011029 (2015).
[13] P. Hořava, Phys. Rev. Lett. **95**, 016405 (2005).
[14] A. P. Schnyder and S. Ryu, Phys. Rev. B. **84**, 060504(R) (2011).
[15] R. Yu, H. M. Weng, Z. Fang, X. Dai, and X. Hu, Phys. Rev. Lett. **115**, 036807 (2015).
[16] Y. Kim, B. J. Wieder, C. L. Kane, and A. M. Rappe, Phys. Rev. Lett. **115**, 036806 (2015).
[17] R. H. Li. X. Y. Cheng, Q. Xie, Y. Sun, D. Z. Li, Y. Y. Li, and X.-Q. Chen, Sci. Rep. **5**, 8446 (2015).
[18] K. K. Wolff, F. Lissner, J. Kohler, and K. Schleid, Eur. J. Inorg. Chem **1**, 92 (2015).
[19] H. J. Zhang, C. X. Liu, X. L. Qi, X. Dai, Z. Fang, and S. C. Zhang, Nat. Phys **5**, 438 (2009).
[20] O. V. Yazyev, J. E. Moore, and S. G. Louie, Phys. Rev. Lett. **105**, 266806 (2010).
[21] P. Larson, V. A. Greanya, W. C. Tonjes, R. Liu, S. D. Mahanti, and C. G. Olsen, Phys. Rev. B. **65**, 085108 (2002).
[22] H. Lin, R. S. Markiewicz, L. A. Wray, L. Fu, M. Z. Hasan, and A. Bansil, Phys. Rev. Lett. **105**, 036404 (2010).
[23] K. Kuroda, M. Ye, A. Kimura, S. V. Eremeev, E. E. Krasovskii, E. V. Chulkov, Y. Ueda, K. Miyamoto, T. Okuda, K. Shimada, H. Namatame, and M. Taniguchi, Phys. Rev. Lett. **105**, 146801 (2010).
[24] C. Niu, Y. Dai, L. Yu, M. Guo, Y. Ma, and B. Huang, Appl. Phys. Lett. **99**, 142502 (2011).
[25] I. P. Rusinov, I. A. Nechaev, and E. V. Chulkov, JEPT. Lett. **98**, 397 (2013).
[26] T. Okuda, T. Maegawa, M. Ye, K. Shirai, T. Warashina, K. Miyamoto, K. Kuroda, M. Arita, Z. S. Aliev, I. R. Amiraslanov, M. B. Babanly, E. V. Chulkov, S. V. Eremeev, A. Kimura, H. Namatame, and M. Taniguchi, Phys. Rev. Lett. **111**, 206803 (2013).
[27] S. V. Eremeev, Yu. M. Kototeev, and E. V. Chulkov, Pis'ma Zh. Eksp. Teor. Fiz. **92**, 183 (2010) [JETP. Lett. **92**, 161 (2010)].
[28] H. Jin, J. H. Song, A. J. Freeman, and M. G. Kanatzidis, Phys. Rev. B **83**, 041202(R) (2011).

[29] I. V. Silkin, Yu. M. Kototeev, S. V. Eremeev, G. Bihlmayer, and E. V. Chulkov, Pis'ma Zh. Eksp. Teor. Fiz. **94**, 234 (2011) [JETP. Lett. **94**, 217 (2011)].
[30] J. Y. Qu, J. K. So, G. Adamo, A. Sulaev, L. Wang, and N. I. Zheludev, Nat. Commun. **5**, 5139 (2014).
[31] Y. Ma, X. Li, L. Kou, B. Yan, C. Niu, Y. Dai, and T. Heine, Phys. Rev. B **91**, 235306 (2015).
[32] J.-J. Zhou, W. X. Feng, Y. Zhang, S. Y. A. Yang, and Y. G. Yao, Sci. Rep. **4**, 3841 (2014).
[33] B. H. Yan, M. Jansen, and C. Felser, Nat. Phys **9**, 709 (2013).
[34] J.-J. Zhou, W. X. Feng, and G.-B. Liu, and Y. G. Yao, New. J. Phys. **17**, 015004 (2015).
[35] J.-J. Zhou, W. X. Feng, C.-C. Liu, S. Guan, S. Y. Yang, and Y. G. Yao, Nano. Lett. **14**, 4767 (2014).
[36] D. Hsieh, D. Qian, L. Wray, Y. Xia, Y. S. Hor, R. J. Cava, and M. Z. Hasan, Nature (London) **452**, 970 (2008).
[37] D. Hsieh, Y. Xia, L. Wray, D. Qian, A. Pal, J. H. Dil, J. Osterwalder, F. Meier, G. Bihlmayer, C. L. Kane, Y. S. Hor, R. J. Cava, and M. Z. Hasan, Science **323**, 919 (2009).
[38] Y. Sun, X.-Q. Chen, S. Yunoki, D. Z. Li, and Y. Y. Li, Phys. Rev. Lett. **105**, 216406 (2010).
[39] T. H. Hsieh, J. W. Liu, and L. Fu, Phys. Rev. B. **90**, 081112 (2014).
[40] W. Feng, D. Xiao, Y. Zhang, and Y. G. Yao, Phys. Rev. B. **82**, 235121 (2010).
[41] D. Xiao, Y. Yao, W. Feng, J. Wen, W. Zhu, X.-Q. Chen, G. M. Stock, and Z. Zhang, Phys. Rev. Lett. **105**, 096404 (2010).
[42] X. Y. Cheng, R. H. Li, Y. Sun, X.-Q. Chen, D. Z. Li, and Y. Li, Phys. Rev. B. **89**, 245201 (2014).
[43] X. Y. Cheng, R. H. Li, D. Z. Li, Y. Y. Li, and X.-Q. Chen, Phys. Rev. B. **92**, 155109 (2015).
[44] X. Y. Cheng, R. H. Li, D. Z. Li, Y. Y. Li, and X.-Q. Chen, Phys. Chem. Chem. Phys. **17**, 6933 (2015).
[45] S. A. Shukarev, M. P. Morozova, and G. V. Kokosh, Zh. Oshch. Khim **26**, 1525 (1956).
[46] R. J. Pleasance, J. Inst. Met. **88**, 45 (1959).
[47] D. G. Schweitzer and J. R. Weeks, ASM. Trans. Q **54**, 185 (1961).
[48] N. N. Zhuravlev and V. P. Melik-Adamyan, Kristallography **6**, 121 (1961).
[49] P. Cucka and C. S. Barrett, Acta Crystallogr. Sect. B **15**, 865 (1962).
[50] N. N. Zhuravlev and E. M. Smirnova, Inorg. Mater **2**, 654 (1966).
[51] B. Eisnmann and K. G. Deller, Z. Naturforsch. Tiel B **30**, 66 (1975).
[52] E. B. Klebanov, O. O. Tvaradze, and A. G. Morachevskii, Tsvetn. Metal. **5**, 126 (1986).
[53] H. OKamoto, *Binary Alloy Phase Diagrams*, edited by T. B. Massalski (ASM International (OH), Ohio, 1990), Vol. 1.
[54] G. Derrien, M. Tillard-Charbonnel, A. Manteghetti, L. Monconduit, and C. Belin, J. Solid State Chem. **164**, 169 (2002).
[55] Y. Wang, J. H. Xin, C. Chen, S. H. Liu, B. Hu, and Y. Du, CALPHAD **45**, 49 (2014).
[56] S. Hösel, Z. Phys. Chem. **219**, 205 (1962).
[57] M. Notin, J. Mejbar, A. Bouhajib, J. Charles, and J. Hertz, J. Alloys Compd. **220**, 62 (1995).
[58] M. P. Smirnov and V. E. Rudnichenko, Russ. J. Inorg. Chem. **8**, 728 (1963).
[59] C. M. Sutton, Solid State Commun. **16**, 327 (1975).
[60] G. Kresse and J. Hafner, Phys. Rev. B. **47**, 558 (1993).
[61] G. Kresse and J. Furthmüller, Comput. Mater. Sci. **6**, 15 (1996).
[62] P. E. Blöchl, Phys. Rev. B. **50**, 17953 (1994).
[63] J. P. Perdew, K. Burke, and M. Ernzerhof, Phys. Rev. Lett. **77**, 3865 (1996).
[64] A. R. Oganov and C. W. Glass, J. Chem. Phys. **124**, 244704 (2006).
[65] A. R. Oganov, H. Stokes, and M. Walle, Acc. Chem. Res. **44**, 227 (2011).
[66] A. O. Lyakhov, A. O. Oganov, H. Stokes, and Q. Zhu, Comput. Phys. Commun. **184**, 1172 (2013).
[67] P. Hohenberg and W. Kohn, Phys. Rev. **136**, B864 (1964).
[68] W. Kohn and L. J. Sham, Phys. Rev. **140**, A1133 (1965).
[69] A. Togo, F. Oba, and I. Tanaka, Phys. Rev. B. **78**, 134106 (2008).
[70] S. Baroni, S. de Gironcoli, A. D. Corso, and P. Giannozzi, Rev. Mod. Phys. **73**, 515 (2001).
[71] J. C. Slater and G. F. Koster, Phys. Rev. **94**, 1498 (1954).
[72] A. A. Mostofi, J. R. Yates, Y.-S. Lee, I. Souza, D. Vanderbilt, and N. Marzari, Comput. Phys. Commun. **178**, 685 (2008).
[73] See Supplemental Materials at http://link.aps.org/supplemental/10.1103/PhysRevB.92.205130 for (I) structural details of binary Sr-Bi compounds, (II) parities of occupied bands at time-reversal invariant momenta, and (III) electronic band structures of $Ca_3Bi_2$ and $Ba_3Bi_2$.
[74] L. Hedin, Phys. Rev. **139**, A796 (1965).
[75] M. S. Hybertsen and S. G. Louie, Phys. Rev. B. **34**, 5390 (1986).
[76] M. Shishkin and G. Kresse, Phys. Rev. B. **74**, 035101 (2006).
[77] L. Fu and C. L. Kane, Phys. Rev. B. **74**, 195312 (2006).
[78] L. Fu, C. L. Kane, E. J. Mele, Phys. Rev. Lett. **98**, 106803 (2007).
[79] R. Yu, W. Zhang, H. J. Zhang, S. C. Zhang, X. Dai, and Z. Fang, Science **329**, 61 (2010).
[80] F. D. M. Haldane, Phys. Rev. Lett. **61**, 2015 (1988).
[81] X. L. Qi, T. L. Hughes, and S. C. Zhang, Phys. Rev. B **78**, 195424 (2008).
[82] C. X. Liu, X. L. Qi, X. Dai, Z. Fang, and S. C. Zhang, Phys. Rev. Lett. **101**, 146802 (2008).
[83] C. Z. Chang, J. S. Zhang, X. Feng, J. Shen, Z. C. Zhang, M. H. Guo, K. Li, Y. B. Ou, P. Wei, L.-L. Wang, Z.-Q. Li, Y. Feng, S. H. Ji, X. Chen, J. F. Jia, X. Dai, Z. Fang, S.-C. Zhang, K. He, Y. Y. Wang, L. Lu, X.-C. Ma, and Q.-K. Xue, Science **340**, 167 (2013).